Manufacturing Multifunctional Vascularized Composites by Through-thickness Frontal Polymerization and Depolymerization: A Numerical Study on the Impact of Sacrificial Fiber Configurations

Zhuoting Chen[a], Xiang Zhang[a,*]

[a]Department of Mechanical Engineering, University of Wyoming, , Laramie, 82071, WY, USA

ARTICLE INFO

Keywords:
Multiphysics modeling
Vascularization
Frontal polymerization
Vascular composites

ABSTRACT

Concurrent through-thickness frontal polymerization and vascularization (FP-VaSC) is emerging as a promising alternative to conventional multi-step fabrication approaches for vascularized thermoset polymers and composites. This method relies on a localized and self-propagating exothermic polymerization reaction front of the polymer matrix, to simultaneously cure the matrix, and depolymerize pre-embedded sacrificial templates. It delivers fully cured thermoset polymers and composites rapidly and energy-efficiently with the desired vascular system in a single step. While previous studies demonstrated the capability of this method for making woven laminates with a single vascular channel created by embedding a single straight sacrificial fiber, it is desirable to explore the potential of this method for making composites with multiple channels for more practical applications. We employ a previously validated thermo-chemical model from our prior study, to systematically investigate the reaction process with the presence of multiple sacrificial fibers. Two sacrificial fiber configurations are considered, namely, inline and staggered fiber configurations. Within each configuration, we consider a range of horizontal and vertical fiber spacing, which also lead to different sacrificial fiber volume fractions. This study reveals the interactions between the sacrificial fiber and the reactions, identifies the working window of this method for different sacrificial fiber configurations, and provides guidance for manufacturing laminates with multiple vascular channels. We also propose an analytical model that can quickly approximate the maximum sacrificial fiber volume fraction that can lead to successful FP-VaSC for a given carbon fiber volume fraction and compare the results with those from the thermo-chemical modeling.

1. Introduction

Biological systems contain vascular pathways that support the retention and transport of fluids and enable multiple and complex functionalities essential to life in dynamic and adverse environments. Bio-inspired vascular composites, with engineered vascular systems embedded in a polymer or polymer composite host, have gained tremendous research interest recently. These vascular systems deliver multiple functionalities, improve the performance and sustainability of the structures, and serve in a variety of engineering fields [1]. For example, engineered vascular systems have been used for healing agent delivery [2–6], energy harvesting and storage [7], and thermal regulation [8]. Thermoset polymer and polymer composites with fiber reinforcement, have been mostly used as the host of vascular networks due to their lightweight, excellent mechanical properties, and outstanding thermal resistance. Manufacturing of vascularized thermoset polymer and polymer composites generally requires a two-step procedure, where a vascular template is first embedded in the host matrix before curing. The host is first cured in an autoclave in the first step, followed by the removal of the sacrificial template in a subsequent step, leaving a clear channel system in the host matrix. Different approaches have been developed to remove the vascular template in the host matrix, including physical removal [9], dissolution [10], and thermal removal by vaporization [11], etc. Among these techniques, the Vaporization of Sacrificial Components (VaSC) has been the most promising technique, which enabled the fabrication of complex and scalable vascular architectures in fiber-reinforced polymer composites for the first time [12]. VaSC first fabricates a sacrificial template made of thermally degradable polymer, which can withstand the curing process of the host matrix without

*Corresponding author
xiang.zhang@uwyo.edu (X. Zhang)
ORCID(s): 0000-0003-0826-4986 (Z. Chen); 0000-0002-7984-6003 (X. Zhang)

depolymerization. The cured parts are then heated at a higher temperature above the depolymerization temperature of the sacrificial template, allowing the template to depolymerize and evaporate, leaving clear channels in the host matrix. VaSC has been demonstrated to successfully manufacture multidimensional vascular systems in polymer and polymer composites [13–15], and achieved multi-functionality suitable for various bio-inspired applications [11, 12, 16].

Recently, frontal polymerization (FP) has emerged as a rapid and energy-efficient curing strategy for manufacturing thermoset polymer and polymer composites [17–19], which also opens up new possibilities for creating vascular systems simultaneously. FP relies on a localized and exothermic polymerization reaction front that, once initiated by a temporal initial stimuli, can self-propagate and cure the monomer thoroughly and rapidly without additional heat input. FP has been reported in several monomers including polyurethanes [20], epoxies [21, 22], acrylates [23, 24], dicyclopentadiene (DCPD) [19], and also works when reinforcements present, enabling the manufacturing of various forms of composite materials [25, 26]. The key aspects FP exhibits such as rapid curing, low energy consumption, and a large amount of heat output offer intriguing potential for integration with other technologies [25, 27–29]. In particular, the exothermic front provides a temperature window that ramps up quickly to its maximum value (e.g., up to 250 ^oC for neat DCPD monomer) as the front approaches, and gradually cools down depending on the environment (e.g., cools to 90 ^oC for neat DCPD monomer exposed in the air at room temperature in few minutes). By designing polymers that could depolymerize and evaporate within the temperature window associated with FP [30], rapid and synchronized fabrication of vascularized thermoset and composites are achieved [31]. In this process, FP is used to simultaneously cure the matrix, and depolymerize the sacrificial template, delivering vascularized polymer and polymer composites in a single process. They have systematically studied, by both experiments and modeling, on how the boundary condition and initial degree of cure of the monomer impact the FP-VaSC process, and demonstrated that complex vascular systems can be manufactured rapidly with minimum energy consumption.

In FP-based curing and depolymerization, front velocity as well as the dimension of the parts along which the front travels, determine the time needed for completing the curing process. In various composite applications such as battery packaging and aerospace engineering, thin-wall structures like shells and plates are heavily used, which feature a much smaller thickness dimension than the in-plane dimensions. Instead of having the front propagating in-plane along the sacrificing channel direction (termed as lateral FP-VaSC), through-thickness FP-VaSC was proposed [32] to fabricate woven composite laminates with straight vascular channel. It was found that depolymerization happens primarily during the cooling down stage of the laminates after the FP completes in the thorough-thickness FP-VaSC. However, the depolymerization front follows the polymerization front with only a small gap in the lateral FP-VaSC. This is because of the reduced amount of energy stored in the system due to the presence of a large volume fraction of carbon fibers (e.g., 30%-60%), as well as the fast completion of FP. This study also signifies the importance of insulation in the manufacturing process, especially for the cases with higher carbon fiber volume fractions for thorough cure and complete VaSC. Based on the findings from both experiments and simulations, woven composites with up to 60% carbon fiber volume fraction and single vascular channel were fabricated, with satisfactory channel geometry and mechanical properties. However, the interaction between the chemical reaction and multiple sacrificial fibers could potentially impact the curing and depolymerization process, and this interaction has not yet been thoroughly understood due to the limited experimental data available which are generally expensive to get.

Multiphysics modeling of FP and FP-based manufacturing processes can help facilitate the understanding of the reaction process, and determine the working window of the manufacturing processes, accelerate and guide the experimental development. Modeling of FP has started from pure monomer system [33, 34], to the incorporation of different fillers [35–38], FP based 3D printing process [28, 29, 39], and concurrent FP and VaSC [31, 32].

The objective of this research is to systematically study the impact of sacrificial fiber configurations on the through-thickness FP-VaSC process, and probe the working window of this manufacturing process. We build on our prior work of thermo-mechanical modeling of through-thickness FP-VaSC [15], considering two different fiber configurations, including the inline and staggered sacrificial fiber configurations. For each configuration, we examine a range of horizontal and vertical fiber spacing, which also leads to different sacrificial fiber volume fractions. We also propose an analytical model that can quickly approximate the maximum sacrificial fiber volume fraction that can lead to successful FP-VaSC for a given carbon fiber volume fraction and compare the results with those from the thermo-chemical modeling. This study reveals the impact of the fiber configuration on the reaction process, identifies the manufacturing space of this method for different fiber configurations, and provides guidance for manufacturing laminates with multiple channels efficiently.

The remainder of the manuscript is organized as follows: Section 2 gives an overview of the thermo-chemical model for FP-VaSC, followed by a systematic study of the through-thickness FP-VaSC in Section 3, where we focus on both

Table 1
Thermal and physical properties of 50 vol % CF/DCPD, Foam plate, and PPC fiber used in the simulation work.

	κ [W/(m·K)]	C_p [J/(kg·K)]	ρ [kg/m^3]	H_r [J/g]
CF	9.36	758	1772	–
DCPD	0.15	1600	980	400
CF/DCPD ($V_f = 50\%$)	0.3	1052	1390	200
Foam	0.03	96	1453	–
PPC	0.25	1313	1800	20

inline and staggered sacrificial fiber arrangements, and study the depolymerization and polymerization characteristics at different fiber spacing, and identify the working window in terms of sacrificing fiber vertical and horizontal spacing. Conclusions are drawn in Section 4.

2. Overview of coupled thermo-chemical modeling of frontal polymerization and depolymerization

The frontal polymerization of host composites and depolymerization of sacrificial polymer fibers are similar coupled thermo-chemical processes, both involve heat transfer and chemical reaction, with the difference that the polymerization releases heat, while the depolymerization absorbs heat. We build on our prior modeling framework for the through-thickness FP-VaSC of sacrificial polypropylene carbonate (PPC) fibers, embedded in CF/DCPD woven composite laminates [32]. This model has been experimentally validated and is employed in the current study. A brief overview of this model is provided here for the completeness of the current manuscript.

In the CF/DCPD composites domain, we track the evolution of temperature, T (in K), and degree of cure α (non-dimensional parameter between 0 and 1, with 0 indicating monomer, and 1 for fully cured polymer), by solving the coupled partial differential equation (PDE)

$$\begin{cases} \nabla \cdot (\bar{\kappa} \nabla T) + \left(1 - V_{\mathrm{f}}\right) \rho_1 H_{r1} \frac{\partial \alpha}{\partial t} = \overline{\rho C_p} \frac{\partial T}{\partial t} \\ \frac{\partial \alpha}{\partial t} = A_1 \exp\left(-\frac{E_1}{RT}\right) (1-\alpha)^{n_1} \alpha^{m_1} \frac{1}{1+\exp[C_1(\alpha - \alpha_{c1} - \alpha_0)]} \end{cases} \tag{1}$$

in which, the heat conduction process is expressed by the first equation with a source term representing the heat generation from the exothermic polymerization reaction, and characterized by the enthalpy H_{r} (in J/kg), and the curing rate $\frac{\partial \alpha}{\partial t}$. Other material properties include the thermal conductivity, density, and specific heat are denoted by κ (in W/(m·K)), ρ (in kg/m^3) and C_{p} (in J/(kg·K)), respectively, and are assumed to be constant during the reaction process. The curing rate, which depends on the current temperature and degree of cure, is described in the second cure kinetics equation, where E (in 1/s) is the activation energy, R is the universal gas constant (in J/(mod·K)), and n, m, C, α_{c} are non-dimensional constants. α_0 represents the initial degree of cure of DCPD in the composite (0.01 in the current study), V_f is the fiber volume fraction in the CF/DCPD composites, subscript '1' indicates properties associated with DCPD, and the overbar denotes the homogenized properties of the CF/DCPD composites. For properties such as density and specific heat, the rule of mixtures considering only the fiber volume fraction provides reasonable estimation, while thermal conductivity needs to further account for the microstructure features. In the current study, the laminates are made of 4.0 mm thickness Toray T300 2 × 2 twill weave carbon fiber plies. This woven fabric composite microstructure can be simplified as a unit cell shown in Fig. 1, following the work from Ning et al. [40]. A closed-form estimation of the homogenized thermal conductivity from their work is adopted, which accounts for all listed geometrical parameters, to compute the thermal conductivity in the transverse direction. The cure kinetics parameters are obtained by fitting an experimental differential scanning calorimetry (DSC) data. All parameters in Eq. (1) are determined in our prior work, and listed in Table 1 and Table 2 for the case of using CF/DCPD composites with 50% fiber volume fraction.

A similar set of coupled thermo-chemical PDE describes the depolymerization process in the sacrificial PPC fiber, with the temperature T and degree of depolymerization β (non-dimensional parameter between 0 and 1, with 0

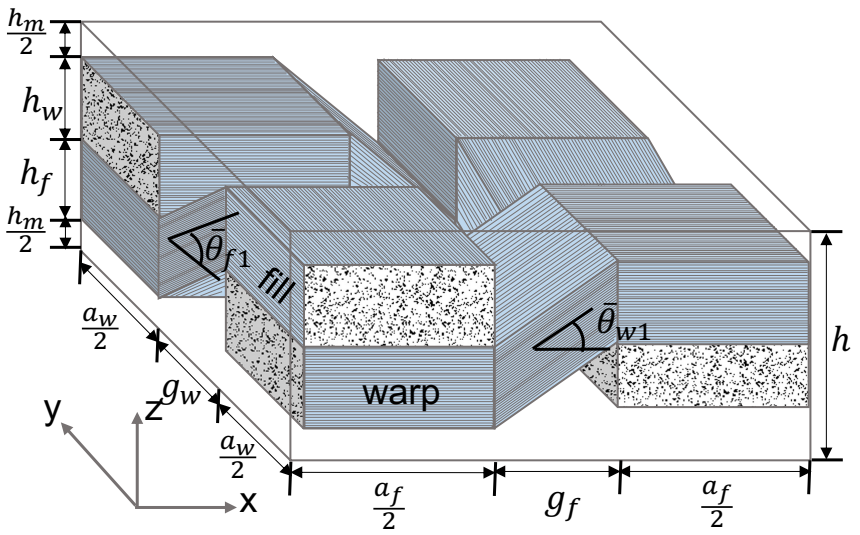

Figure 1: The idealized unit cell of the woven composite model. h and h_m are the thickness of the unit cell and matrix layer, respectively. h_w,h_f denote the thickness of the warp and fill yarn, respectively. a_w, a_f respectively represent the width of the warp and fill yarn. g_w and g_f respectively mean gap width of the warp and fill yarn. $\bar{\theta}_{w1}$, $\bar{\theta}_{f1}$ indicate the mean fiber inclination angle in the warp and fill direction.

Table 2
Cure kinetics of DCPD and PPC fiber used in the simulation work.

	A [1/s]	E [KJ/mol]	n	m	α_c	C
DCPD	2.53×10^{17}	115	4.05	0.85	0.4	15.36
PPC	6.18×10^{12}	108	0.98	0.3	–	–

indicating intact ppc fiber, 1 for fully depolymerized state) as unknowns

$$\begin{cases} \nabla \cdot \left(\kappa_2 \nabla T\right) - \rho_2 H_{r2} \frac{\partial \beta}{\partial t} = \rho_2 C_{p2} \frac{\partial T}{\partial t} \\ \frac{\partial \beta}{\partial t} = A_2 \exp\left(-\frac{E_2}{RT}\right)(1-\beta)^{n_2} \beta^{m_2} \end{cases} \tag{2}$$

where the main difference from Eq.(1) is that the depolymerization absorbs heat as indicated by the minus sign in front of the source term in the diffusion equation, and subscript "2" is used to indicate the parameters for PPC fiber. The depolymerization kinetic parameters are obtained by fitting an experimental Thermogravimetric Analysis (TGA) data and determined in our prior work [32] All parameters in Eq. (2) are determined in our prior work, and listed in Table 1 and Table 2.

In the current study, we consider the specimen being sandwiched by two tool foam plates on the top and bottom, same as prior experimental study [32]. In the foam plates, only a heat diffusion problem is solved (i.e., similar to the first equation in Eq. 1 and (2), without the heat source term), with all properties for the foam tool plate provided in Table 1. To account for the heat convection from the tool plate to the air, we apply convection heat transfer coefficient $h = 25W/(m^2)$, with the initial temperature of the CF/DCPD composites, PPC, and tool plates all equal to the room temperature of 25^oC.

2.1. Simulation domain

The coupled thermo-chemical model in equations (1) and (2) are solved using the open-source C++ finite element solver - Multiphysics Object-Oriented Simulation Environment (MOOSE) [41]. MOOSE features an implicit Euler time-stepping scheme, the pre-conditioned Jacobian-free Newton-Krylov scheme, and an adaptive mesh refinement scheme, which is suitable for solving this highly transient and nonlinear FP and VaSC process. In our previous work,

we simplified the modeling process by looking at the cross-section perpendicular to the single PPC fiber, and the model was experimentally validated [32]. In the current work, we account for the presence of multiple PPC fibers and aim to understand the impact of PPC fiber configurations on the FP-VaSC process and explore the working window of through-thickness FP-VaSC. We focus on two types of PPC fiber configurations. The first is an inline configuration where the PPC fibers are arranged in equally spaced rows and columns where each row is parallel to the plies. The second is a staggered configuration, where the neighboring column is shifted in the vertical direction such that in the vertical direction, the PPC fiber in the neighboring row is in the middle of the two PPC fibers in the neighboring columns. In both cases, the horizontal and vertical spacing are used to characterize the PPC configuration. For computational efficiency, we still consider a rectangular area of a repeating unit of the wet layup cross section in the y-z plane as shown in Fig. 2a. Due to the repetitive nature of the chosen domain in the y direction, both vertical sides are considered to be adiabatic. The total thickness (H) of the simulation domain is 4.0 mm, the total length (L) varies with fiber configuration and the diameter of PPC fiber is 0.4 mm. While the inline sacrificial fiber arrangement model uses half of the repeating unit due to symmetry, the staggered sacrificial fiber arrangement model is the exact simulation domain. The details of the configurations are shown in Fig. 2a. For each configuration, different horizontal and vertical spacing are considered. All of the models use the standard quadrilateral element with an element size 0.052×0.052 mm. Two examples of the meshes are given in Fig. 2b. This inline model has 24,266 elements with 25,341 nodes and half of the domain is used due to symmetry. The staggered model has 48,564 elements with 49,663 nodes in the domain.

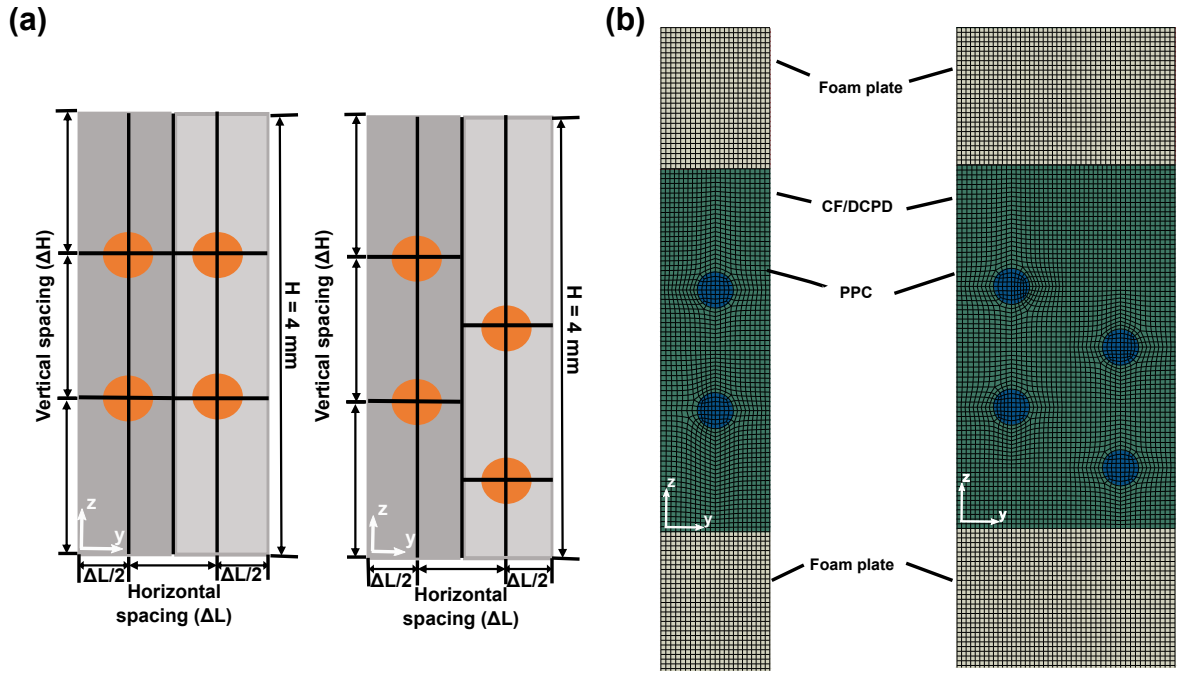

Figure 2: (a) Schematics of the inline and staggered sacrificial fiber configurations, (b) example mesh of the two configurations. Note that half of the domain is used in the simulation of the inline case due to symmetry.

3. Impact of sacrificing fiber configurations

A systematic analysis of the impact of sacrificing fiber configurations on the FP-VaSC process is conducted, focusing on the inline and staggered configuration of the sacrificing fibers by varying horizontal and vertical spacing. It is expected that if the horizontal and vertical spacing becomes too small, an unstable front, as well as incomplete depolymerization of the sacrificial fiber, may happen, and this study aims to identify the working window of complete through thickness FP-VaSC.

3.1. Inline fiber configuration

In this section, a series of models with inline sacrificial fiber arrangement is established to study the FP-VaSC under different horizontal and vertical spacing, ranging from 0.5 - 1.2 mm, and 0.57 - 1.33 mm, respectively. This range is chosen such that the spacing is higher than sacrificing fiber diameter (no sacrificial fiber overlapping), and wide enough that allows us to probe the working window for successful through-thickness FP-VaSC.

An example simulation with $\Delta H \times \Delta L = 0.66 \times 1.2$ mm spacing, which achieves successful FP-VaSC with sacrificial fiber volume fraction of 13.1% is chosen for detailed analysis. The evolution of conversion (i.e., both cure and depolymerization) is shown in Fig. 3. The polymerization front initiates at about $t = 27$ s, and it takes about 5 s for the front to go around the first row of PPC fibers. The front then propagates for another 8 s and reaches the middle of the laminates. However, it only takes 3 s to go through the remaining half domain, indicating an increasingly faster front propagation. Slower polymerization between two sacrificial fibers is also observed, especially at the top row of sacrificial fibers as shown for $t = 42.8$ s in Fig. 3. This slower polymerization is due to excessive heat absorption by the two sacrificial fibers during their depolymerization. The depolymerization starts from the top row of the sacrificial fibers, 6 s after the curing front arrives at the top surface of the host matrix (i.e., $t = 49$ s). It then propagates in the reverse direction with the polymerization front (i.e., from the top to the bottom), and completes within 6 minutes. The lack of synchronization between FP and VaSC is mainly due to the relatively low front temperature at this high fiber volume fraction, and also the fast completion of FP due to small laminates thickness, as found from our prior study [32].

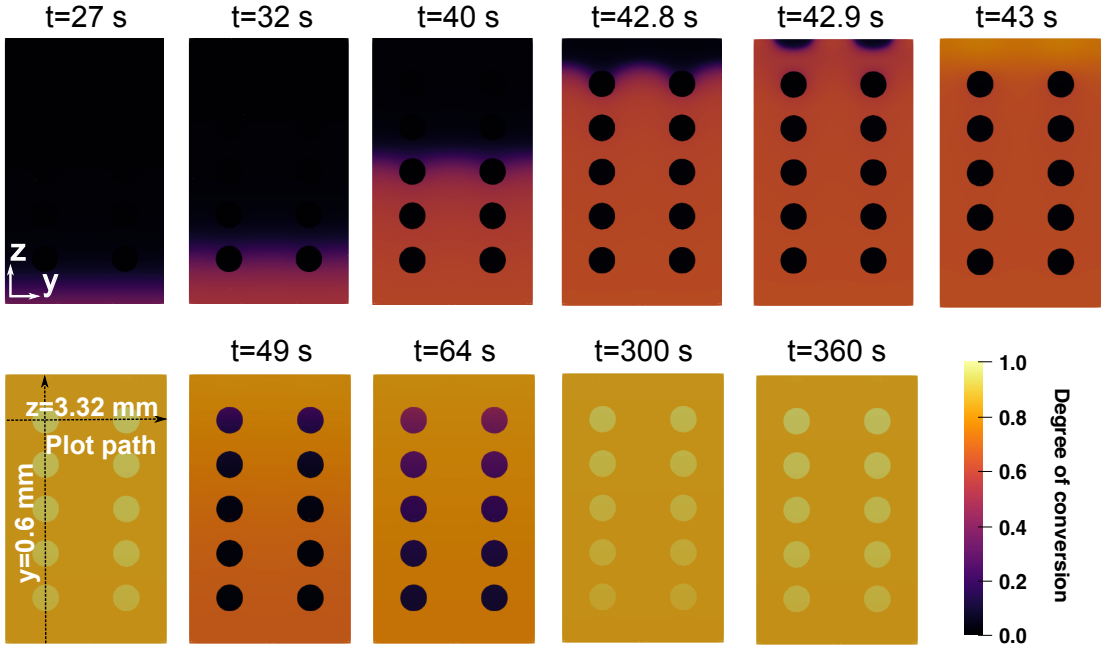

Figure 3: Degree of cure and depolymerization contours at different times of inline fiber configuration with vertical space of 0.66 mm and horizontal space of 1.2 mm.

To understand the causes of faster frontal polymerization at the top, and the reverse depolymerization direction, the temperature and degree of reaction distributions are further examined by plotting their values along the vertical line passing through the center of the left column of sacrificial fibers in Fig. 4. It is observed that even before the front reaches the top (i.e., before $t = 43$ s), the temperature at the top has an obvious increase (e.g., from 30 to 45 ^oC at time 42.8 s). This temperature increase in the laminates before FP is due to the heating from the reaction at the bottom through the relatively high thermal conductivity of the composites at the current fiber volume fraction. This heating, together with the insulative tool plate on the top, leads to the much higher front temperature at the top as shown in Fig. 4a, causing faster front propagation and depolymerization to happen first at the top and then to the bottom side as shown in Fig. 3. The high front temperature at the top also leads to a higher degree of cure at the top when FP finishes

as shown in Fig. 4b. As time continues, the temperature distribution becomes uniform rapidly within the laminates, due to the high thermal conductivity of the composite as shown in Fig. 4c. The polymerization process continues as the system cools down and by $t = 360\ s$, the degree of cure reaches 0.85, as shown in Fig. 4b.

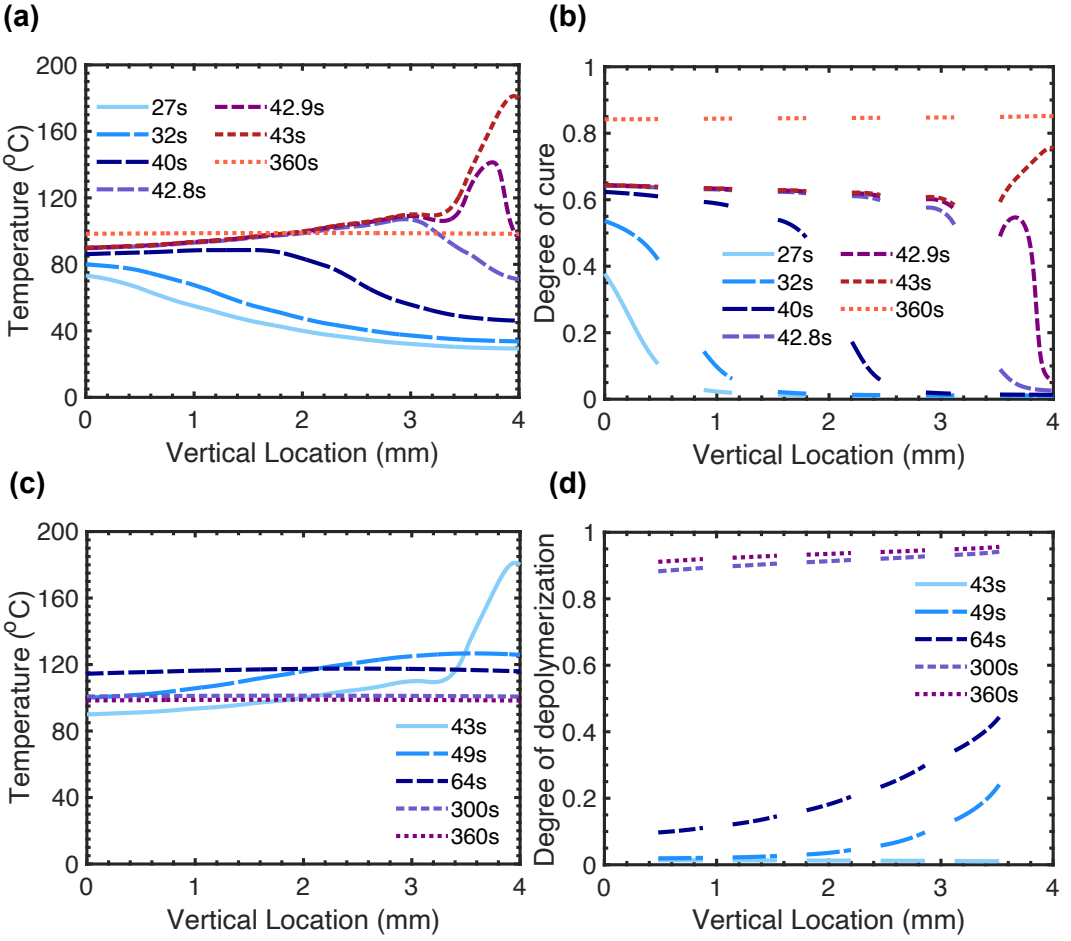

Figure 4: Evolution and distribution of (a) Temperature from 27 – 360 s,(b) Degree of cure from 27 – 360 s,(c) Temperature from 43 – 360 s, (d) Degree of depolymerization from 43 – 360 s, during FP-VaSC along a vertical line passing through the center of the left column of sacrificial fiber (i.e., y = 0.6 mm) of inline fiber configuration with vertical space of 0.66 mm and horizontal space of 1.2 mm.

The degree of depolymerization evolution in Fig. 4d further confirms that depolymerization indeed lags behind frontal polymerization, and mostly takes place after the frontal polymerization during the cooling down without the presence of a depolymerization front. This observation verifies the importance of insulation and the slow cooling stage in the depolymerization, which aligns with our prior work [32]. When the system fully cools down, depolymerization reaches a degree of 0.90 and above, with a slight increase from the bottom to the top as shown in Fig. 4d. This level of depolymerization is considered successful VaSC, based on our previously established criteria of equal or greater than 0.90 [32].

Figure 5 shows the temperature and degree of reaction distributions along a horizontal line at $z = 3.32$ mm, which is across the center of the top row of sacrificial fibers. In general, the temperature in sacrificial fiber is lower than that in the composite, and also lower in the middle of the fiber than that in the outer region, since the depolymerization process absorbs heat. The temperature and degree of cure of composites are lower in areas close to fibers, and higher in areas away from the fibers (e.g., see Fig. 5a, b). While the PPC fibers continuously absorb heat, the temperature of the fibers increases for a short period of time (e.g., between $t = 43$ s and 49 s) and cools down along with composites

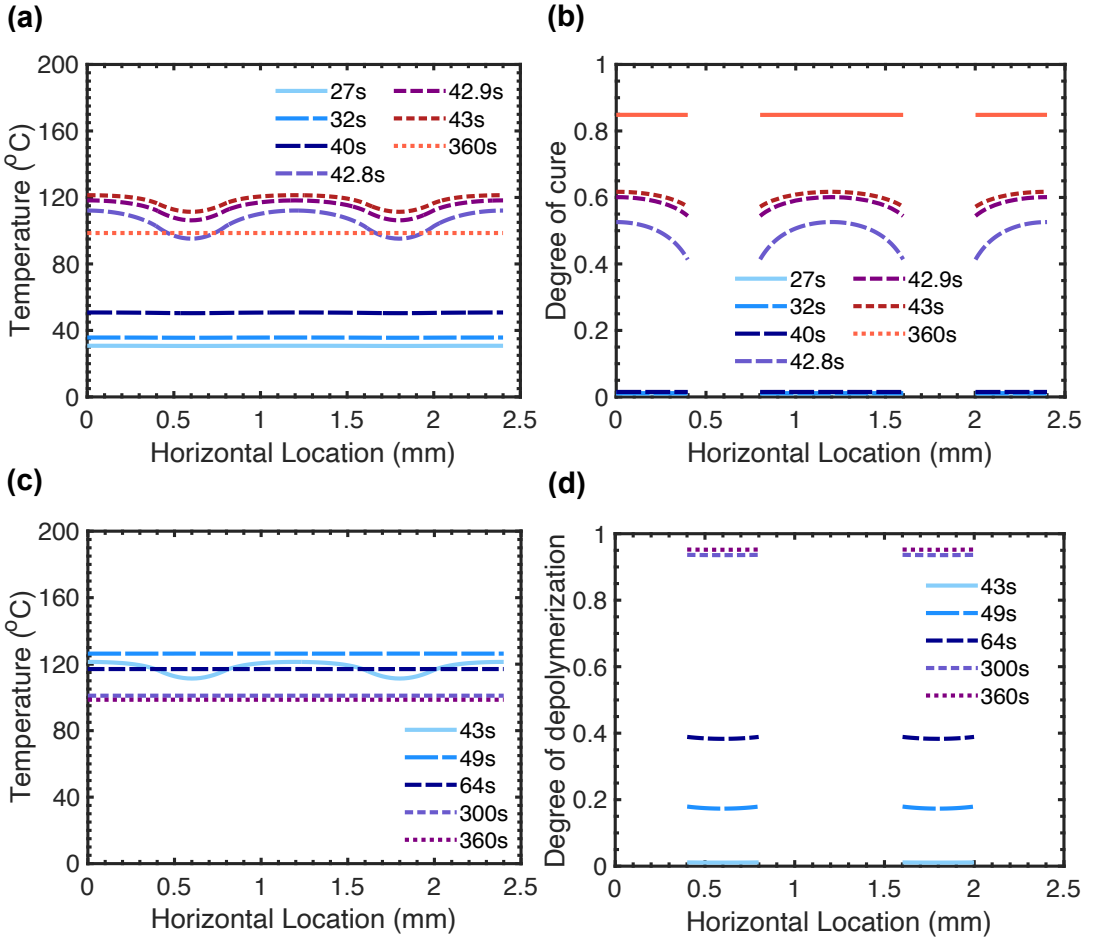

Figure 5: Evolution and distribution of (a) Temperature from 27 – 360 s, (b) Degree of cure from 27 – 360 s, (c) Temperature from 43 – 360 s, (d) Degree of depolymerization from 43 – 360 s, during FP-VaSC along horizontal line passing through the center of the top row of sacrificial fiber (i.e., z = 3.32 mm) of inline fiber configuration with vertical space of 0.66 mm and horizontal space of 1.2 mm.

shown in Fig. 5c. Accordingly, the degree of depolymerization starts with a slightly higher value in the outer part but eventually becomes uniform in the fiber due to uniform temperature.

To fully probe the working window of through-thickness FP-VaSC for the current woven laminates with 50% fiber volume fraction, a series of simulations with varying horizontal and vertical spacing are conducted. If a chosen spacing leads to complete FP (i.e., degree of cure reaches 0.85) and VaSC (i.e., degree of depolymerization reaches 0.90) within a specific time limit, we consider this spacing to be a working case for that manufacturing time limit. We choose three different time limits to quantify the working window for the through-thickness FP-VaSC, including 5 minutes, 10 minutes, and 15 minutes, which are much shorter than conventional vascular composite manufacturing time [31]. The degree of conversion of different spacing at the three chosen time limits are presented in Fig. 6, and the times of front reaching the top surface as well as the start of depolymerization are compiled in Fig. 7. Successful FP-VaSC cases by the specified time limit are enclosed by the red line, indicating the working window of the through-thickness FP-VaSC. It is found that vascularization with sparse fiber arrangement is a rapid process while a more compact sacrificial fiber case needs a much longer time to start and complete the depolymerization, and eventually will result in unsuccessful manufacturing, mainly due to incomplete depolymerization of the sacrificial fibers. The narrowest spacing (i.e., along the boundary of the working window) that leads to successful FP-VaSC within 15 min are $\Delta H \times \Delta L = 0.57$ mm x 1.20 mm, 0.66 mm x 1.00 mm which correspond to sacrificial fiber volume fraction of 15.7%, and 1.00 mm x 0.75 mm,

1.33 mm x 0.50 mm which correspond to sacrificial fiber volume fraction of 12.6%, respectively. It should be noted that if we allow a longer manufacturing time, more compact spacing may allow successful manufacture. However, we limit our consideration to only up to 15 minutes to leverage the great potential of through-thickness FP-VaSC.

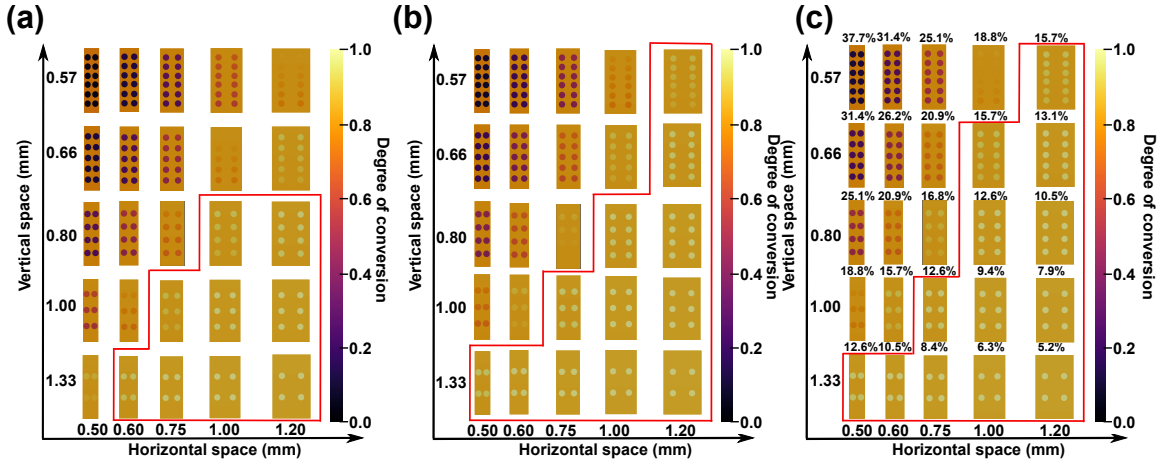

Figure 6: Manufacturing space of inline fiber configuration with different horizontal and vertical spaces between fibers within (a) 5 min,(b) 10 min, and (c) 15 min. Numbers in (c) indicates the corresponding sacrificial fiber volume fractions.

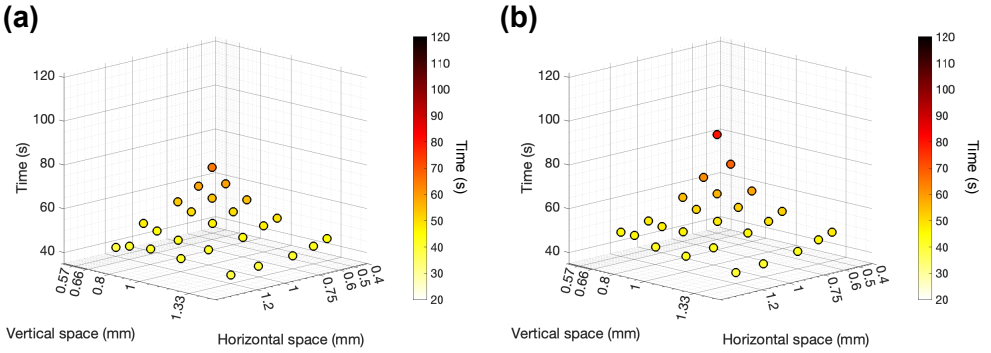

Figure 7: (a) Time of front propagates to the top surface of composites, (b) Time of fibers start to depolymerize, of inline fiber configuration with different horizontal and vertical spaces between fibers. Color of each data point indicates the temperature at the time specified.

To understand the failure in through-thickness FP-VaSC, a simulation of a case located right outside the working window is chosen for detailed analysis. This case has vertical space of 0.80 mm, and horizontal space of 0.75 mm, corresponding to the second row and the second column of Fig. 6. After 15 minutes, the degree of cure and depolymerization distributions along a vertical line at y = 0.375 mm (i.e., passing through the center of the first column of sacrificial fibers) are plotted in Fig. 8a. The curing process evenly leads to a degree of cure around 0.82. The degree of depolymerization is above 0.90 of the upper channel and below 0.90 of lower channel, which suggests a partial depolymerization. Figure 8b shows the degree of cure evolution at the middle of the composite and depolymerization evolution at the middle of the chosen vertical line. Similar to the full FP-VaSC case, depolymerization starts after the curing as shown in Fig. 8b, and the temperature the sacrificial fiber experiences at the top is higher than that at the bottom shown in Fig. 8c, eventually leads to difference in the degree of depolymerization among the fibers. These results suggest that one needs to pay particular attention to the bottom sacrificial fibers when examining the success of the FP-VaSC.

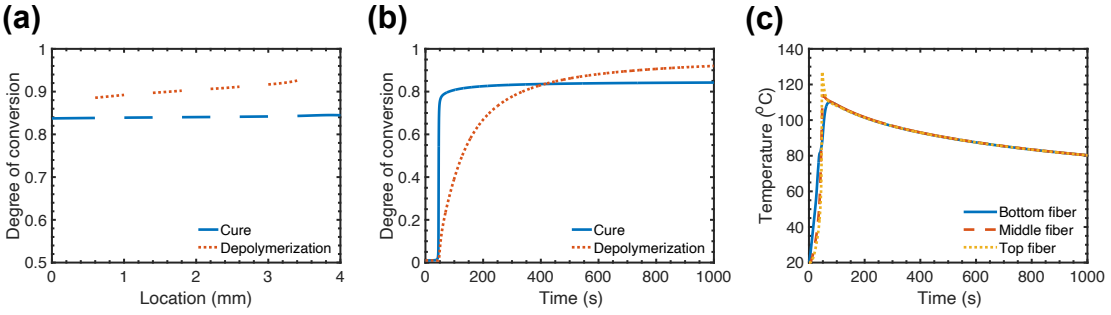

Figure 8: Simulation of inline fiber configuration with vertical space of 0.80 mm and horizontal space of 0.75 mm. (a) Degree of cure and depolymerization distribution along the line y = 0.375 mm after 15 min, (b) Degree of cure profile at the location,y = 0.75 mm, z = 3.2 mm,and degree of depolymerization profile at the location,y = 0.375 mm, z = 3.2 mm, (c) Temperature evolution of three fibers located at bottom, middle, top of the composites, respectively.

3.2. Staggered fiber configuration

Simulations with staggered fiber configuration accounting for a wide range of horizontal (0.4 - 1.2 mm), and vertical (0.57 - 1.33 mm) spacing are conducted. A case with the same spacing (i.e., vertical spacing 0.66 mm, horizontal spacing 1.20 mm) and sacrificial fiber volume fraction (i.e., 13.1%) as the inline case in Section 3.1 is analyzed here. Figure 9 shows the evolution of the degree of cure and depolymerization. Compared to the inline configuration case in Fig. 3, the front also initiates at 27 s but propagates slower over the bottom half of the domain. Then, the front propagates very fast through the top part of the domain. It should be noted that due to the staggering arrangement of the PPC fibers, the top PPC fiber in the left column is closer to the top surface of the laminate, causing the polymerization to finish first on the right, and then moves to the left side. In this case, the PPC fibers are fully depolymerized within 5 minutes. Although the front travels unevenly, the curing and depolymerization speed in this case is faster than the inline case.

Temperature and degree of reaction distributions along the vertical line passing through the center of the left column sacrificial fibers and the horizontal line passing the center of the top row sacrificial fiber are provided in Fig. 10 and Fig. 11, respectively. In Fig. 10a, it is evident that the temperature at the top of the laminate increases even further at 42.9 s compared to the inline configuration case due to the staggering positions of fibers. The corresponding degree of cure in this area is higher, which indicates the temperature elevation accelerates the curing process (Fig. 10b). The temperature maintained over 170 řC in the composites vicinity (Fig. 10c). This slower cooling period of the composite subsequently speeds up the depolymerization of the fibers. The degree of depolymerization is over 0.90 throughout the fibers domain at 5 min (Fig. 10d).

In the horizontal direction, a reduced temperature near the fiber results in a lower degree of cure as seen from Fig. 11a, b. This occurs because the fiber absorbs heat from the surrounding composite. A slightly higher temperature persists in the right region until depolymerization initiates, attributed to the lower-positioned fiber on the right side of the laminate. Once the curing front reaches the top surface of the composite, the fiber heats up and starts depolymerization. After 49 s, fiber cools in conjunction with the composite (as depicted in Fig. 11c) and further depolymerizes within the cooling stage (Fig. 11d).

Particularly, at 42.8 s, distinct front behaviors around the top row fibers and the top boundary surface of the composite can be attributed to the temperature distributions. The temperature contours for both inline and staggered fiber configurations are presented in Fig. 12. In the inline configuration (Fig. 12a), the top PPC fibers maintain an equal distance from the top surface of the composite and evenly disperse the heat released by the composite. Conversely, in the staggered configuration (as depicted in Fig. 12), only the left fiber absorbs heat, causing heat concentration on the right side. This concentration results in a higher temperature in the right region, consequently accelerating the front propagation within this composite zone. The accelerated front propagation not only enhances the overall curing speed but also expedites the depolymerization process.

Since the fiber positions of the staggered fiber configuration model, the horizontal space, as defined, can be narrower than the inline fiber configuration case. The smallest horizontal space is chosen as 0.4 mm, which is the diameter of the fiber. Figure 13 provides the manufacture predictions of staggered fiber configuration. Overall, the staggered fiber

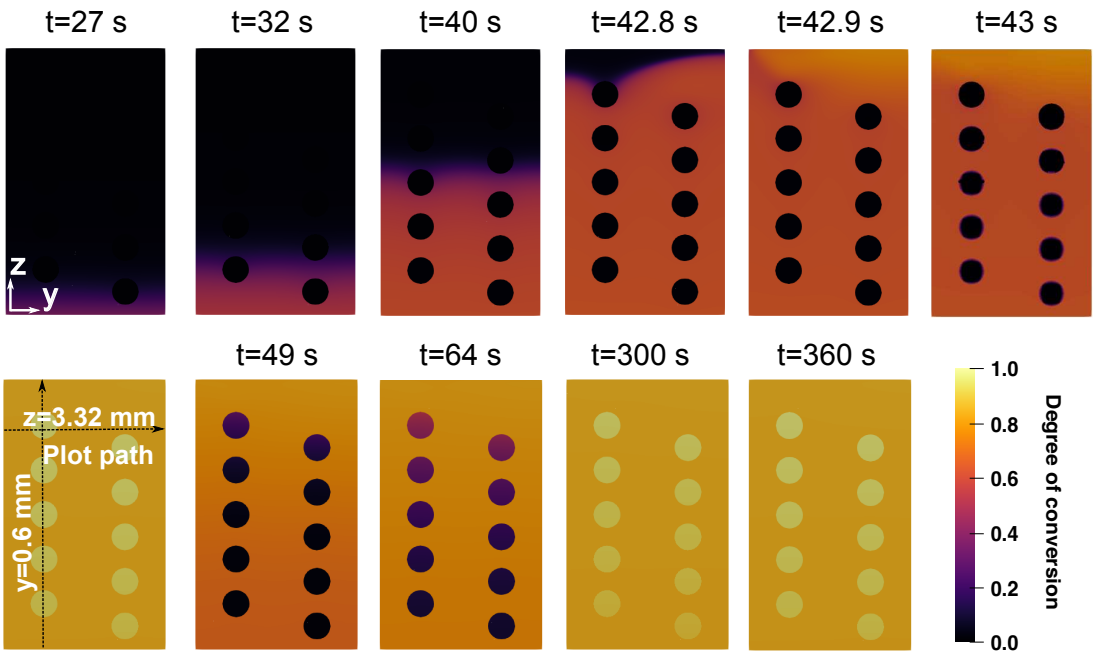

Figure 9: Degree of cure and depolymerization contours at different times of staggered fiber configuration with vertical space of 0.66 mm and horizontal space of 1.20 mm.

configuration allows larger manufacturing space than the inline case under three time constraints. Most simulations have shown completion of cure, while the completion of depolymerization varies. Within 15 min, compared to the inline case, the narrowest spacing (i.e., along the boundary of the working window) are $\Delta H \times \Delta L$ = 0.57 mm x 1.20 mm, 0.66 mm x 1.00 mm, 1.00 mm x 0.60 mm and 1.33 mm x 0.40 mm, which correspond to a sacrificial fiber volume fraction of 15.7%, and 0.80 mm x 0.75 mm which corresponds to a sacrificial fiber volume fraction of 16.8%, respectively (Fig. 13c). To accomplish wider manufacturing space and higher efficiency, the staggered fiber configuration is recommended under certain demand.

The entire fabrication of staggered fiber configuration is faster than the inline configuration, however knowing time of each stage is still critical as a prediction for future production, especially for the tighter geometry system. The time predictions with different fiber spaces are provided in Fig. 14. Similar pattern as the inline configuration can be observed from the staggered case. The time of front arrives top surface of the composite increases gradually while the starting time of depolymerization significantly delays when shorten both spaces, which also matches previous findings in Fig. 13 and proves our view in section 3.1. Although the fiber configurations are closely related to the front propagation, both the inline and staggered configurations show smoother curing than depolymerization, especially when the sacrificial fiber spacing are small. Despite this substantial time expenditure for extremely contracted geometry, within certain threshold of spaces, staggered configuration facilitates the manufacturing process.

3.3. An analytical model for estimating maximum sacrificial fiber volume fraction for successful through-thickness FP-VaSC

We have investigated the through-thickness FP-VaSC of a 50% carbon fiber volume fraction under different horizontal and vertical spacing for both the inline and staggered sacrificial fiber configurations and determined the working window for a given manufacturing time limit. While we can use the same method to study the case of different carbon fiber volume fractions, it is desirable to develop an analytical model that can easily determine the maximum sacrificial fiber volume fraction for a given carbon fiber volume fraction and time limit with reasonable accuracy.

As an approximation, we can assume that all sacrificial fibers experience the same temperature history regardless of the configuration. As we observe that the laminates quickly reach a relatively uniform temperature after the reaction

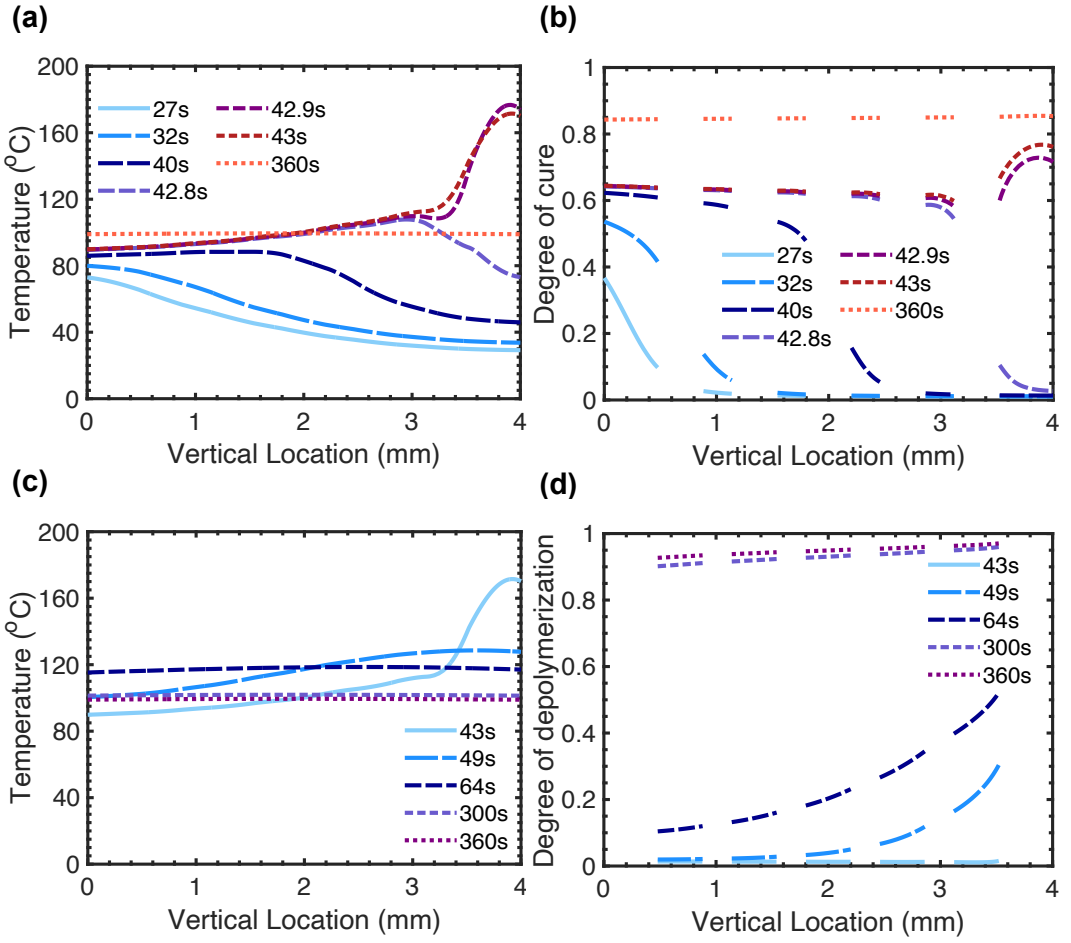

Figure 10: Evolution and distribution of (a) Temperature from 27 – 360 s,(b) Degree of cure from 27 – 360 s,(c) Temperature from 43 – 360 s, (d) Degree of depolymerization from 43 – 360 s, during FP-VaSC along vertical line passing through the center of the left column of sacrificial fibers (i.e., y = 0.6 mm) of staggered fiber configuration with vertical space of 0.66 mm and horizontal space of 1.20 mm.

(about 1 minute as shown in Fig. 5 and 11), and then slowly cool down (i.e., about 5 ^oC/min for the current laminates) due to convective heat loss to the environment. If the temperature starts with an approximated value T (i.e., the uniform temperature after FP) one minute after the start of the process, and reduces at a rate of 5 ^oC/min (i.e., the cooling rate), the corresponding evolution of the degree of depolymerization under this prescribed temperature history can be computed by the so-called 0D model, which uses an implicit time integration to solve the depolymerization kinetics in Eq. (2). FP-VaSC is considered successful when the degree of depolymerization reaches 0.90. The starting temperature that allows full depolymerization within a chosen manufacturing time limit can be obtained from the 0D model. We choose to study the manufacturing time limits of 5, 10, and 15 minutes, corresponding to 4, 9 and 14 minutes of prescribed temperature history. The starting temperatures required to finish VaSC are $T_1 = 118.54^oC$, $T_2 = 116.86^oC$, $T_3 = 116.75^oC$, respectively.

The temperature of the composites after FP and VaSC can be approximated by assuming all the heat release and absorption due to the chemical reaction happens instantaneously and thoroughly, which takes the form

$$T = T_0 + \frac{\left(1 - V_p\right)\left(1 - V_f\right)\left(1 - \alpha_0\right)\rho_1 H_{r1} - V_p \rho_2 H_{r2}}{V_p \rho_2 C_{p2} + \left(1 - V_p\right)\left(\left[1 - V_f\right)\rho_1 C_{p1} + V_f \rho_f C_{pf}\right]} \tag{3}$$

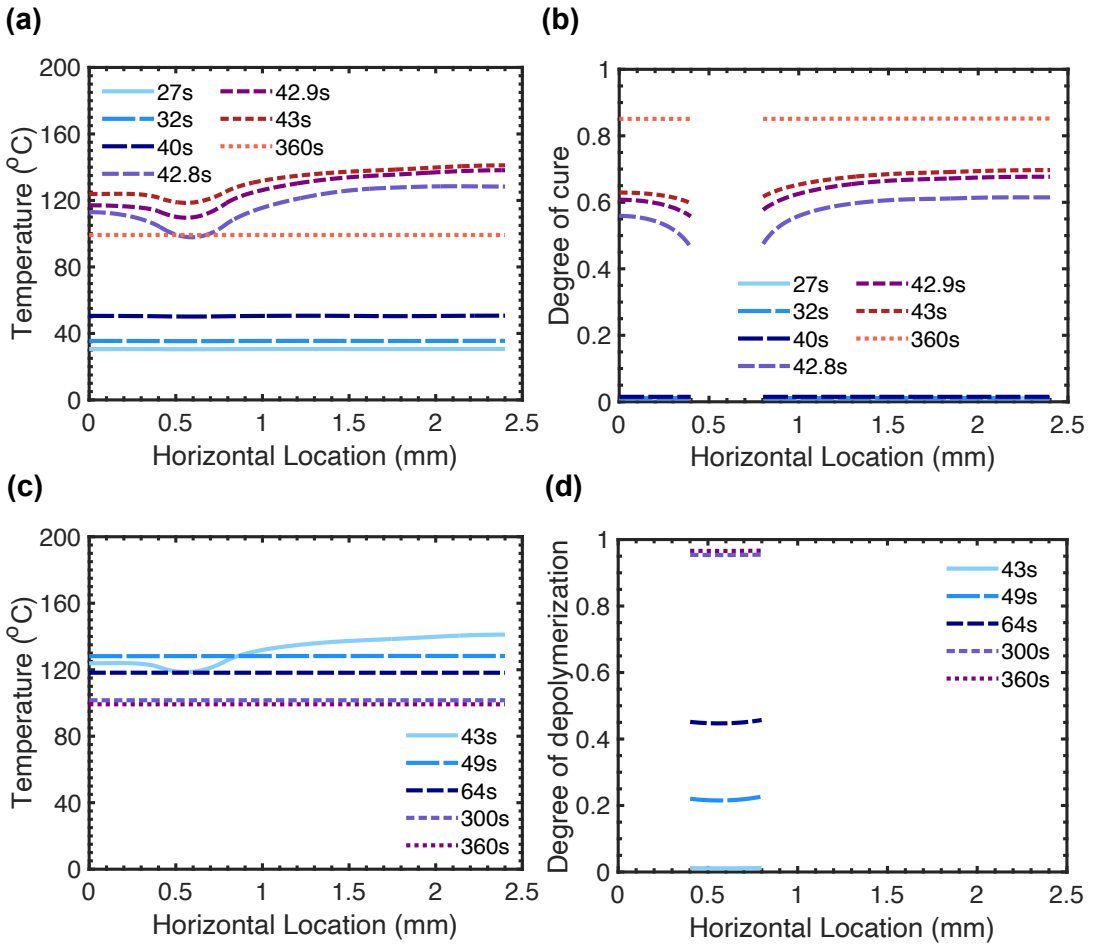

Figure 11: Evolution and distribution of (a) Temperature from 27 – 360 s,(b) Degree of cure from 27 – 360 s;(c) Temperature from 43 – 360 s, (d) Degree of depolymerization from 43 – 360 s, during FP-VaSC along horizontal line z = 3.32 mm of staggered fiber configuration with vertical space of 0.66 mm and horizontal space of 1.20 mm.

where T_0 is the initial temperature of the system (in řC, set at 20 řC in this work), and V_f indicates the volume fraction of carbon fibers in the composite, V_p denotes the volume fraction of PPC fibers (i.e., volume fraction of the composite is then (1-V_p)). The subscript 1 denotes the properties of the DCPD resin, 2 represents the properties of the PPC fiber, and f denotes the properties of the carbon fiber. The properties used in this equation are presented in Table 1. By enforcing the temperature T in Eq. (3) to be T_1, T_2 and T_3 for a given carbon fiber volume fraction, we can compute the maximum sacrificial fiber volume fractions that can complete FP-VaSC in 5, 10 and 15 minutes. The predictions are plotted in Fig. 15.

Overall, as the carbon fiber volume fraction increases, the maximum sacrificial fiber volume fraction that leads to successful VaSC decreases, which is due to lower enthalpy in the system and lower front temperature. The starting temperatures needed for the manufacturing time limits of 10 and 15 minutes are very close, which is because the depolymerization becomes very slow when the degree of depolymerization is high and the temperature is low, which also suggests it is not meaningful to consider even longer manufacturing time.

The maximum sacrificial fiber volume fractions predicted from the simulations in Section 3 for both the inline and staggered configuration at 50% carbon fiber volume fraction to achieve successful FP-VaSC in 5, 10, and 15 minutes are also marked in the plot. It is found that the maximum sacrificial fiber volume fraction from the analytical model is slightly higher than that predicted by the full-field model, as it does not account for the sacrificial and front interaction. This assumption is responsible for the discrepancy between the full-field simulations results and that from

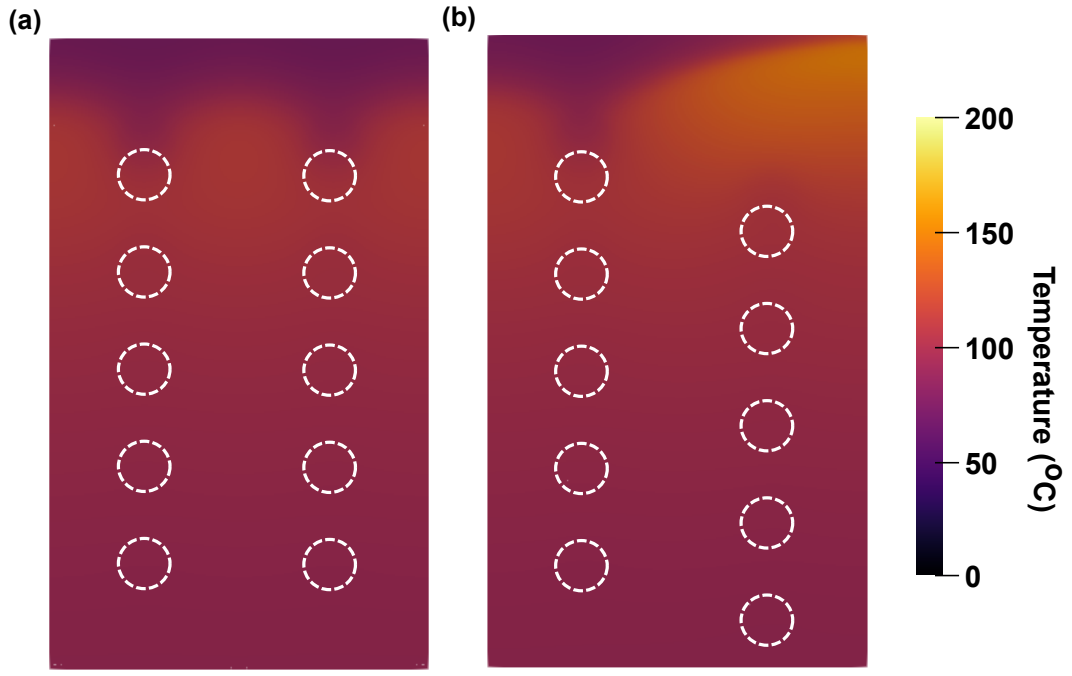

Figure 12: Temperature distribution at t=42.8 s of (a) inline and (b) staggered fiber configurations with vertical space of 0.66 mm and horizontal space of 1.20 mm.

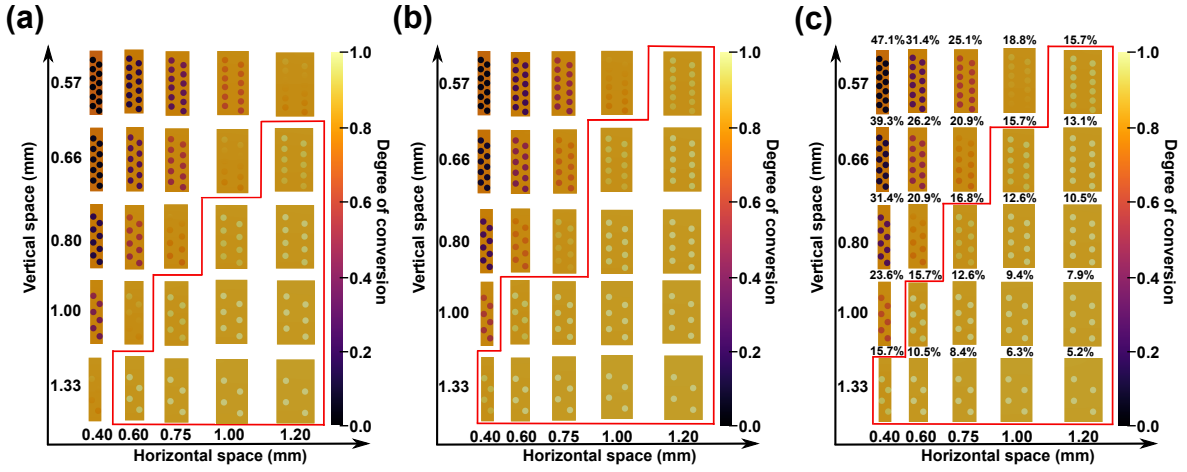

Figure 13: Manufacturing space of staggered fiber configuration with different horizontal and vertical spaces between fibers at (a) 5 min,(b) 10 min,(c) 15 min, respectively. Numbers in (c) indicates the corresponding sacrificial fiber volume fractions.

the analytical model as shown in Fig. 15, which are considered reasonable. To pinpoint smallest horizontal and vertical spacing in both sacrificial fiber configurations, one could use the analytical model to obtain a quick estimation of the maximum sacrificial fiber volume fraction. From there, only a few full-field simulations are needed to obtain the smallest sacrificial fiber spacing that allow successful FP-VaSC. It should be also noted that the analytical model is not dependent on V_f and sacrificial fiber configurations, so it is expected to apply it to other V_f as well. Besides, the staggered configuration allows a higher sacrificial fiber volume fraction compared to the inline configuration. Overall,

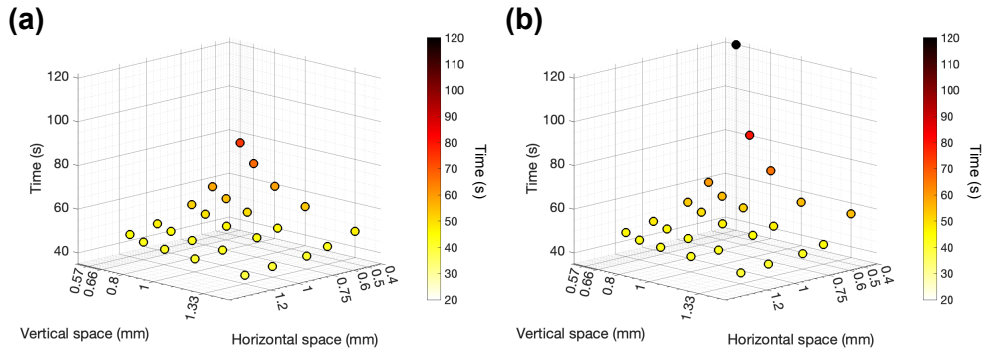

Figure 14: (a) Time of front propagates to the top surface of composites, (b) Time of fibers start to depolymerize, of staggered fiber configuration with different horizontal and vertical spaces between fibers.

the analytical model provides a reasonable estimation considering its simplicity. For a specific complex vascular system (e.g., a cooling system with branching), there would be cases where either some sacrificial fibers have much larger diameters and branch into multiple smaller sacrificial fibers, or some sacrificial fibers may change direction. Under these cases, the local V_f and V_p may change. A full-field simulation is needed to capture the interaction between the front and the local features, the analytical model may not work well in these cases.

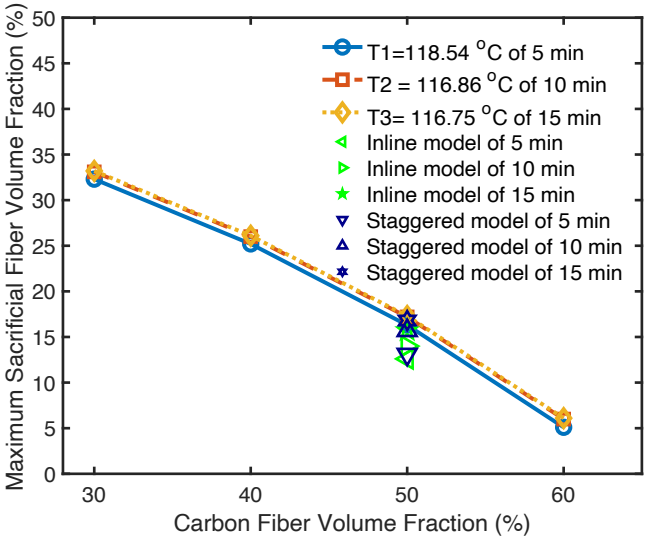

Figure 15: Maximum sacrificial fiber at different V_f comparison between prediction model and simulation.

4. Conclusions

In this manuscript, we employed an experimental validated coupled thermo-chemical model from our prior study to investigate the impact of sacrificial fiber configuration on polymerization and depolymerization during the through-thickness FP-VaSC. Two configurations of the sacrificial fibers are considered, namely, inline and staggered fiber configurations. For each configuration, we consider a range of horizontal and vertical fiber spacing, which also leads to different sacrificial fiber volume fractions. This study reveals the interactions between the sacrificial fiber and the reaction processes, identifies the working window of this method for different sacrificial fiber configurations,

and provides guidance for manufacturing laminates with multiple vascular channels. To be more specific, the major conclusions we draw from the study include:

1. The curing of composite is less challenging compared to the vascularization of embedded sacrificial fibers. The curing is completed on the order of seconds, while the depolymerization will start after the polymerization and take minutes or longer to finish during the cool-down stage of the composites. The time needed for full depolymerization of the sacrificial fiber increases nonlinearly and dramatically when the sacrificial fiber spacing becomes smaller. This suggests that we could use more insulative tooling to achieve faster manufacturing for the case with large sacrificial fiber spacing.
2. The degree of depolymerization of the sacrificial fibers at different locations along the thickness direction of the laminates varies, and is normally higher close to the top surface of the laminates and lower close to the bottom surface. This is mainly because of the heating of the top portion and thermal spikes generated when the front reaches the top surface. When multiple rows of sacrificial fibers are embedded, careful examination of the depolymerization of the fibers close to the bottom surface is critical to ensure full depolymerization.
3. Overall, the staggered sacrificial fiber configuration can potentially support a higher sacrificial fiber volume fraction. In our 50% carbon fiber composites case, the inline configuration can support up to 15.7% sacrificial fiber volume fraction, while the staggered configuration can support up to 16.8% sacrificial fiber volume fraction.
4. Our analytical model, which only accounts for sacrificial fiber volume fraction but not the fiber configuration, provides a fast and acceptable estimation of the maximum sacrificial fiber volume fraction allowed.

5. Acknowledgement

This work has been funded by the Wyoming NASA EPSCoR, NASA Grant #80NSSC19M0061. The high-performance computing resources and support from the Advanced Research Computing Center (ARCC) at the University of Wyoming are also greatly acknowledged.

CRediT authorship contribution statement

Zhuoting Chen: Writing review & editing, Writing original draft, Visualization, Validation, Software, Methodology, Investigation, Formal analysis, Data curation. **Xiang Zhang:** Writingreview & editing, Supervision, Resources, Project administration, Methodology, Funding acquisition, Conceptualization.

References

[1] N. Sottos, S. White, I. Bond, Introduction: self-healing polymers and composites, Journal of The Royal Society Interface 4 (13) (2007) 347–348.
[2] S. R. M. Paladugu, P. R. Sreekanth, S. K. Sahu, K. Naresh, S. A. Karthick, N. Venkateshwaran, M. Ramoni, R. A. Mensah, O. Das, R. Shanmugam, A comprehensive review of self-healing polymer, metal, and ceramic matrix composites and their modeling aspects for aerospace applications, Materials 15 (23) (2022) 8521.
[3] E. N. Brown, S. R. White, N. R. Sottos, Microcapsule induced toughening in a self-healing polymer composite, Journal of Materials Science 39 (5) (2004) 1703–1710.
[4] T. J. Swait, A. Rauf, R. Grainger, P. B. Bailey, A. D. Lafferty, E. J. Fleet, R. J. Hand, S. A. Hayes, Smart composite materials for self-sensing and self-healing, Plastics, Rubber and Composites 41 (4-5) (2012) 215–224.
[5] E. B. Murphy, F. Wudl, The world of smart healable materials, Progress in Polymer Science 35 (1-2) (2010) 223–251.
[6] S. R. White, P. H. Geubelle, Get ready for repair-and-go, Nature Nanotechnology 5 (4) (2010) 247–248.
[7] C. A. Aubin, S. Choudhury, R. Jerch, L. A. Archer, J. H. Pikul, R. F. Shepherd, Electrolytic vascular systems for energy-dense robots, Nature 571 (7763) (2019) 51–57.
[8] B. D. Kozola, L. A. Shipton, V. K. Natrajan, K. T. Christensen, S. R. White, Characterization of active cooling and flow distribution in microvascular polymers, Journal of Intelligent Material Systems and Structures 21 (12) (2010) 1147–1156.
[9] C. Norris, I. Bond, R. Trask, Interactions between propagating cracks and bioinspired self-healing vascules embedded in glass fibre reinforced composites, Composites Science and Technology 71 (6) (2011) 847–853.
[10] J. S. Miller, K. R. Stevens, M. T. Yang, B. M. Baker, D.-H. T. Nguyen, D. M. Cohen, E. Toro, A. A. Chen, P. A. Galie, X. Yu, et al., Rapid casting of patterned vascular networks for perfusable engineered three-dimensional tissues, Nature Materials 11 (9) (2012) 768–774.
[11] J. Patrick, K. Hart, B. Krull, C. Diesendruck, J. Moore, S. White, N. Sottos, Continuous self-healing life cycle in vascularized structural composites, Advanced Materials 26 (25) (2014) 4302–4308.
[12] A. P. Esser-Kahn, P. R. Thakre, H. Dong, J. F. Patrick, V. K. Vlasko-Vlasov, N. R. Sottos, J. S. Moore, S. R. White, Three-dimensional microvascular fiber-reinforced composites, Advanced Materials 23 (32) (2011) 3654–3658.
[13] M. Ziaee, I. Naseri, J. W. Johnson, K. A. Franklin, M. Yourdkhani, Frontal polymerization and three-dimensional printing of thermoset polymers with tunable thermomechanical properties, ACS Applied Polymer Materials.

[14] I. Naseri, M. Yourdkhani, Rapid and energy-efficient frontal curing of multifunctional composites using integrated nanostructured heaters, ACS Applied Materials & Interfaces 14 (44) (2022) 50215–50224.
[15] P. Centellas, M. Yourdkhani, S. Vyas, B. Koohbor, P. Geubelle, N. Sottos, Rapid multiple-front polymerization of fiber-reinforced polymer composites, Composites Part A: Applied Science and Manufacturing 158 (2022) 106931.
[16] H. Dong, A. P. Esser-Kahn, P. R. Thakre, J. F. Patrick, N. R. Sottos, S. R. White, J. S. Moore, Chemical treatment of poly (lactic acid) fibers to enhance the rate of thermal depolymerization, ACS applied materials & interfaces 4 (2) (2012) 503–509.
[17] J. A. Pojman, Traveling fronts of methacrylic acid polymerization, Journal of the American Chemical Society 113 (16) (1991) 6284–6286.
[18] J. A. Pojman, V. M. Ilyashenko, A. M. Khan, Free-radical frontal polymerization: self-propagating thermal reaction waves, Journal of the Chemical Society, Faraday Transactions 92 (16) (1996) 2825–2837.
[19] I. D. Robertson, M. Yourdkhani, P. J. Centellas, J. E. Aw, D. G. Ivanoff, E. Goli, E. M. Lloyd, L. M. Dean, N. R. Sottos, P. H. Geubelle, et al., Rapid energy-efficient manufacturing of polymers and composites via frontal polymerization, Nature 557 (7704) (2018) 223–227.
[20] S. Fiori, A. Mariani, L. Ricco, S. Russo, First synthesis of a polyurethane by frontal polymerization, Macromolecules 36 (8) (2003) 2674–2679.
[21] A. Mariani, S. Bidali, S. Fiori, M. Sangermano, G. Malucelli, R. Bongiovanni, A. Priola, UV-ignited frontal polymerization of an epoxy resin, Journal of Polymer Science Part A: Polymer Chemistry 42 (9) (2004) 2066–2072.
[22] S. Scognamillo, C. Bounds, S. Thakuri, A. Mariani, Q. Wu, J. A. Pojman, Frontal cationic curing of epoxy resins in the presence of defoaming or expanding compounds, Journal of Applied Polymer Science 131 (11).
[23] C. Nason, T. Roper, C. Hoyle, J. A. Pojman, UV-induced frontal polymerization of multifunctional (meth) acrylates, Macromolecules 38 (13) (2005) 5506–5512.
[24] Y. Gao, F. Shaon, A. Kumar, S. Bynum, D. Gary, D. Sharp, J. A. Pojman, P. H. Geubelle, Rapid frontal polymerization achieved with thermally conductive metal strips, Chaos: An Interdisciplinary Journal of Nonlinear Science 31 (7) (2021) 073113.
[25] M. Ziaee, J. W. Johnson, M. Yourdkhani, 3D printing of short-carbon-fiber-reinforced thermoset polymer composites via frontal polymerization, ACS Applied Materials & Interfaces 14 (14) (2022) 16694–16702.
[26] Y. Gao, S. Li, J.-Y. Kim, I. Hoffman, S. K. Vyas, J. A. Pojman, P. H. Geubelle, Anisotropic frontal polymerization in a model resin–copper composite, Chaos: An Interdisciplinary Journal of Nonlinear Science 32 (1) (2022) 013109.
[27] Q. Li, H.-X. Shen, C. Liu, C.-f. Wang, L. Zhu, S. Chen, Advances in frontal polymerization strategy: From fundamentals to applications, Progress in Polymer Science (2022) 101514.
[28] J. E. Aw, X. Zhang, A. Z. Nelson, L. M. Dean, M. Yourdkhani, R. H. Ewoldt, P. H. Geubelle, N. R. Sottos, Self-regulative direct ink writing of frontally polymerizing thermoset polymers, Advanced Materials Technologies (2022) 2200230.
[29] Z. Chen, M. Ziaee, M. Yourdkhani, X. Zhang, Multiphysics modeling of frontal polymerization-assisted layer-by-layer additive manufacturing of thermoset polymer components, Additive Manufacturing 59 (2022) 103182.
[30] M. Garg, A. C. Ladd, J. E. Aw, X. Zhang, N. R. Sottos, Sacrificial cyclic poly (phthalaldehyde) templates for low-temperature vascularization of polymer matrices, ACS Applied Polymer Materials 4 (1) (2021) 479–487.
[31] M. Garg, J. E. Aw, X. Zhang, P. J. Centellas, L. M. Dean, E. M. Lloyd, I. D. Robertson, Y. Liu, M. Yourdkhani, J. S. Moore, et al., Rapid synchronized fabrication of vascularized thermosets and composites, Nature Communications 12 (1) (2021) 1–9.
[32] P. Centellas, M. Garg, Z. Chen, X. Zhang, N. Parikh, P. Geubelle, N. Sottos, Energy-efficient manufacturing of multifunctional vascularized composites, Journal of Composite Materials (2022) 00219983221142353.
[33] E. Goli, I. D. Robertson, P. H. Geubelle, J. S. Moore, Frontal polymerization of dicyclopentadiene: a numerical study, The Journal of Physical Chemistry B 122 (16) (2018) 4583–4591.
[34] D. Devadoss, J. A. Pojman, V. Volpert, Mathematical modeling of thiol-ene frontal polymerization, Chemical engineering science 61 (4) (2006) 1261–1275.
[35] Y. Wang, Modeling the through-thickness frontal polymerization of unidirectional carbon fiber thermoset composites: Effect of microstructures, Journal of Applied Polymer Science 139 (31) (2022) e52735.
[36] E. Goli, N. A. Parikh, S. K. Vyas, X. Zhang, N. R. Sottos, J. S. Moore, P. H. Geubelle, Manufacturing of carbon-and glass-fiber composites using frontal polymerization, in: International Conference on Composite Materials (22nd: 2019: Melboune, VIC.), Engineers Australia Melbourne, VIC, 2019, pp. 1509–1517.
[37] S. Vyas, X. Zhang, E. Goli, P. Geubelle, Frontal vs. bulk polymerization of fiber-reinforced polymer-matrix composites, Composites Science and Technology 198 (2020) 108303.
[38] S. Vyas, E. Goli, X. Zhang, P. Geubelle, Manufacturing of unidirectional glass-fiber-reinforced composites via frontal polymerization: A numerical study, Composites Science and Technology 184 (2019) 107832.
[39] Z. Chen, M. Ziaee, M. Yourdkhani, X. Zhang, Coupled thermo-chemical modeling of frontal polymerization-assisted additive manufacturing of thermoset polymer components, in: AIAA SCITECH 2023 Forum, 2023, p. 0317.
[40] Q.-G. Ning, T.-W. Chou, A closed-form solution of the transverse effective thermal conductivity of woven fabric composites, Journal of Composite Materials 29 (17) (1995) 2280–2294.
[41] A. D. Lindsay, D. R. Gaston, C. J. Permann, J. M. Miller, D. Andrš, A. E. Slaughter, F. Kong, J. Hansel, R. W. Carlsen, C. Icenhour, L. Harbour, G. L. Giudicelli, R. H. Stogner, P. German, J. Badger, S. Biswas, L. Chapuis, C. Green, J. Hales, T. Hu, W. Jiang, Y. S. Jung, C. Matthews, Y. Miao, A. Novak, J. W. Peterson, Z. M. Prince, A. Rovinelli, S. Schunert, D. Schwen, B. W. Spencer, S. Veeraraghavan, A. Recuero, D. Yushu, Y. Wang, A. Wilkins, C. Wong, MOOSE: Enabling massively parallel multiphysics simulation, SoftwareX 20 (2022) 101202.